Contrib Mineral Petrol (2004) 148: 489–501
DOI 10.1007/s00410-004-0620-0

ORIGINAL PAPER

B. Chen · B. M. Jahn · Y. Arakawa · M. G. Zhai

Petrogenesis of the Mesozoic intrusive complexes from the southern Taihang Orogen, North China Craton: elemental and Sr–Nd–Pb isotopic constraints

Received: 2 June 2004 / Accepted: 1 September 2004 / Published online: 2 October 2004

Abstract A geochemical and isotopic study was carried out for three Mesozoic intrusive suites (the Xishu, Wu'an and Hongshan suites) from the North China Craton (NCC) to understand their genesis and geodynamic implications. The Xishu and Wu'an suites are gabbroic to monzonitic in composition. They share many common geochemical features like high Mg# and minor to positive Eu anomalies in REE patterns. Initial Nd–Sr isotopic compositions for Xishu suite are $\varepsilon_{Nd}(135\ Ma) = -12.3$ to -16.9 and mostly $I_{Sr} = 0.7056$–0.7071; whereas those for Wu'an suite are slightly different. Pb isotopic ratios for Xishu suite are $(^{206}Pb/^{204}Pb)_i = 16.92$–$17.3$, $(^{207}Pb/^{204}Pb)_i = 15.32$–$15.42$, $(^{208}Pb/^{204}Pb)_i = 37.16$–$37.63$, which are slightly higher than for Wu'an suite. The Xishu–Wu'an complexes are considered to originate from partial melting of an EM1-type mantle source, followed by significant contamination of lower crustal components. The Hongshan suite (mainly syenite and granite) shows distinctly higher $\varepsilon_{Nd}(135\ Ma)$ values (-8 to -11) and slightly higher Pb isotopic ratios than the Xishu–Wu'an suites. It was formed via fractionation of a *separate* parental magma that also originated from the EM1-type mantle source, with incorporation of a small amount of lower crustal components. Partial melting of the mantle sources took place in a back-arc extensional regime that is related to the subduction of the paleo-Pacific slab beneath the NCC.

Editorial Responsibility: J. Hoefs

B. Chen (✉)
School of Earth and Space Sciences, Peking University, Beijing, 100871, China
E-mail: binchen@pku.edu.cn

B. M. Jahn
Department of Geosciences, National Taiwan University, Taipei, 106, Taiwan

B. Chen · Y. Arakawa
Institute of Geosciences, The University of Tsukuba, Ibaraki-ken, 305-8572, Japan

M. G. Zhai
Institute of Geology and Geophysics, Chinese Academy of Sciences, Beijing, 100029, China

Introduction

Several interesting issues concerning the evolution of the subcontinental lithospheric mantle (SCLM) beneath the eastern NCC have been investigated by many workers in the last decade (Menzies et al. 1993; Menzies and Xu 1998; Xu 2001; Gao et al. 2002; Chen and Zhai 2003). The occurrence of diamonds in Paleozoic kimberlites implies the presence of a thick (150–220 km), and refractory lithospheric keel underlying the craton, while mantle xenoliths in Cenozoic basalts suggest a thin (60–120 km), and fertile oceanic-type lithosphere in the Cenozoic (Song et al. 1990; Xu 2001). Such a change of lithospheric nature implies a significant erosion of the ancient lithospheric mantle (Archaean in age; Gao et al. 2002) during the Mesozoic, and distinguishes the NCC from most other ancient cratons. The lithosphere thinning was coupled with widespread Mesozoic magmatism. What is the origin of the Mesozoic magmatism and how was it related to the lithospheric mantle evolution? What geodynamic setting change caused the sudden surge of the Mesozoic magmatism in the NCC? Understanding to these issues has been significantly hindered by lack of systematic studies on Mesozoic magmatism. In this paper, we present the results of elemental and Nd–Sr–Pb isotopic data for Mesozoic intrusive complexes from the southern Taihang orogen (Fig. 1) in eastern NCC. They will be used to trace the source of these rocks, and investigate the relationship between Mesozoic magmatism and lithospheric mantle evolution.

Geological setting and sample description

The geological setting of the NCC has been frequently described (e.g., Jahn et al. 1988; Menzies et al. 1993). The NCC is one of the oldest continental nuclei in the world, with basement of mainly Archaean to Early Proterozoic gneisses (Jahn et al. 1988). Thick sequences

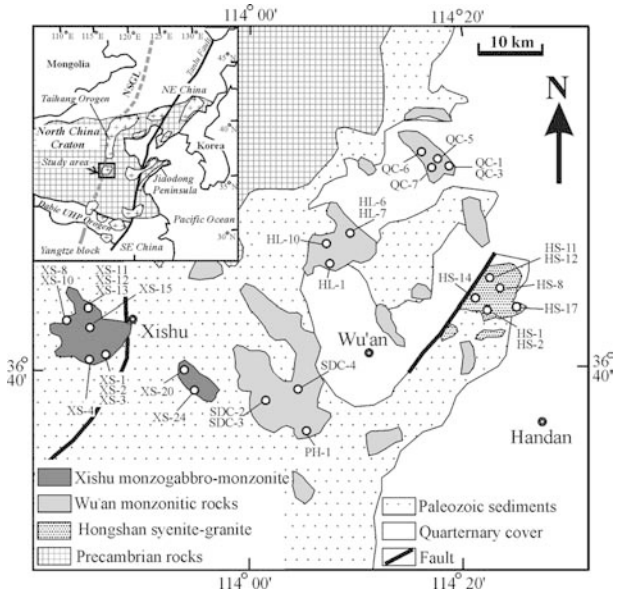

Fig. 1 Geological sketch map of the southern Taihang orogen. *Inset* shows distribution of the Mesozoic magmatic rocks (*cross*) in eastern North China craton (*chessboard*). *NSGL* south–north gravity lineament

of middle to late Proterozoic sediments unconformably overlie the basement rocks, indicating that the craton was stabilized by the early Proterozoic at about 1.8 Ga, and much of the craton remained stable up to Triassic time. However, the eastern part of the NCC (to the east of a south–north gravity lineament; inset of Fig. 1) was intensely remobilized since early Mesozoic, with a thin lithosphere (60–120 km) and widespread Mesozoic magmatism and basin development. This is in contrast with a thick (150–220 km) lithosphere and rare magmatism in the region to the west of the lineament. The southern margin of the NCC is the Dabie ultra-high pressure (UHP) orogen that was formed during the process of a Triassic collision between the Yangtze block and NCC (Chen et al. 2002a; inset of Fig. 1).

Three suites of Mesozoic intrusions occur in the southern Taihang orogen: the Xishu monzogabbro–monzonite, the Wu'an monzonite–quartz monzonite, and the Hongshan syenite–granite (Fig. 1). Peridotite xenolths occur as enclaves in the Xishu rocks (Xu and Lin 1991). Brief petrological description for the main rock types is given below.

Monzogabbros are medium-grained, dark green rocks, made up of clinopyroxene (20%), hornblende (25%), biotite (5%), plagioclase (40, with An = 59-50) and K-feldspar (8%), and accessory phases like titanomagnetite and zircon. Monzodiorites are richer in plagioclase (55%) and K-feldspar (15%), and poorer in clinopyroxene (5–10%) than monzogabbros. Monzonites mainly contain plagioclase (45%) and K-feldspar (35–40%), and small amounts of hornblende, clinopyroxene, magnetite, titanomagnetite, allanite, sphene, apatite and zircon. Syenites are pinkish-grey porphyritic rocks, containing phenocrysts of plagioclase and K-feldspar in a medium- to fine-grained groundmass. Main constituent mineral is K-feldspar (60–85%); other minerals include plagioclase (5–15%), quartz (< 5%) and mafic phases such as hornblende (5–10%), biotite (5%) and clinopyroxene (5–10%), and accessory apatite, titanomagnetite, allanite, zircon and sphene.

The emplacement time for the intrusives of the Taihang orogen was dated at 129–138 Ma using the zircon U–Pb and Rb–Sr whole-rock isochron methods (Davis et al. 1998; Cai et al. 2003). This is consistent with a new zircon U–Pb age of 127 ± 1 Ma for a diorite pluton from the Xishu suite (Peng et al. 2004). Thus, emplacement of the magmatic complexes in the Taihang orogen took place in the period of 138–125 Ma.

Analytical methods

Chemical and isotopic analyses were conducted in the Institute of Geology and Geophysics (IGG, Beijing). Major elements were analyzed using XRF, with analytical uncertainty < 3%. Trace elements were measured using ICP-MS; samples were digested by acid (HF + $HClO_4$) in bombs. Analytical uncertainties are 10% for elements with abundances < 10 ppm, and around 5% for those > 10 ppm (Table 1).

Nd–Sr–Pb isotopic analyses were also measured at the IGG (Beijing). Some of the samples were chosen for duplicate analyses of Rb–Sr and Sm–Nd isotopes in Rennes (France) to cross-check the data quality, and the results obtained from the two laboratories appear in good agreement (Table 2). Details of the analytical methods in Rennes can be found in an earlier report (e.g., Chen et al. 2002a). In Beijing, samples were dissolved using acid (HF + $HClO_4$) in sealed Savillex beakers on a hot plate for a week. Separation of Rb, Sr and light REE was done using a cation-exchange column (packed with Bio-Rad AG50Wx8 resin). Sm and Nd were further purified using a second cation-exchange column, conditioned and eluded with dilute HCl. Mass analyses were performed using a multi-collector VG354 mass spectrometer as described by Qiao (1988). Rb, Sr, Sm and Nd concentrations were measured using the isotopic dilution method. $^{87}Sr/^{86}Sr$ ratios were normalized against $^{86}Sr/^{88}Sr = 0.1194$. $^{143}Nd/^{144}Nd$ ratios were normalized against $^{146}Nd/^{144}Nd = 0.7219$. $^{87}Sr/^{86}Sr$ ratios were adjusted to NBS-987 Sr standard = 0.710250, and the $^{143}Nd/^{144}Nd$ ratios to La Jolla Nd standard = 0.511860. The uncertainty in concentration analyses by isotopic dilution is ± 2% for Rb, ± 0.5–1% for Sr, and < ± 0.5% for Sm and Nd depending upon concentration levels. The overall uncertainty for Rb/Sr is ± 2% and Sm/Nd ± 0.2–0.5%. Procedural blanks are: Rb = 120 pg, Sr = 200 pg, and Nd = 50–100 pg. For Pb isotope analyses, sample powder was spiked and dissolved in concentrated HF at 800°C for 72 h. Lead was separated and purified by conventional anion-exchange technique (AG1×8, 200–400 resin) with diluted HBr. Isotopic ratios were measured using the VG-354 mass

Table 1 Chemical analyses for rocks from the south Taihang orogen, North China

Sample	HS-1	HS-2	HS-8	HS-14	HS-17	HS-11	HS-12	QC-1	QC-3	QC-5	QC-6	QC-7	SDC-2	SDC-3	SDC-4	HL-1	HL-6	HL-7	HL-10	PH-1	XS-1	XS-2	XS-3	XS-4	XS-8	XS-10	XS-11	XS-12	XS-13	XS-15	XS-20	XS-24
Rock	syen	syen	syen	syen	syen	gran	gran	mz	q.mz	mz	dio	dio	q.mz	q.mz	mz	mz	mz.di	mz.di	dio	mz	mz	gbb	gbb	gbb	mz	mz.di	mz	mz.di	mz.di	mz.di	mz.di	gbb
wt%																																
SiO_2	63.19	66.91	65.34	61.48	63.14	74.11	75.67	58.66	63.99	58.72	57.11	54.05	62.14	61.08	57.35	59.69	56.64	63.85	59.94	60.21	57.79	50.08	51.71	50.14	58.54	52.24	61.43	60.33	57.24	57.77	56.31	51.18
TiO_2	0.36	0.24	0.15	0.45	0.38	0.07	0.07	0.6	0.29	0.61	0.48	0.78	0.47	0.57	0.61	0.56	0.73	0.47	0.53	0.52	0.61	0.92	0.83	0.93	0.66	0.79	0.54	0.50	0.80	0.62	0.69	0.72
Al_2O_3	15.66	17.51	18.25	16.38	17.1	12.66	11.53	15.64	16.79	15.67	13.46	15.87	16.01	15.95	16.43	17.03	16.62	18.42	16.79	17.04	15.91	15.52	15.48	14.66	16.19	15.16	17.32	17.56	17.13	16.03	16.49	12.9
FeO	4.76	1.43	1.03	5.44	3.57	1.99	2.07	6.86	3.79	7.02	4.78	8.02	4.84	6.04	7.44	4.14	7.02	1.09	5.69	5.95	7.28	10.52	10.15	11.58	7.26	9.27	2.66	5.06	3.00	7.32	3.33	8.79
MnO	0.10	0.01	0.01	0.09	0.06	0.06	0.08	0.10	0.05	0.08	0.06	0.08	0.05	0.09	0.11	0.06	0.063	0.01	0.06	0.08	0.12	0.14	0.16	0.17	0.11	0.13	0.04	0.06	0.09	0.12	0.08	0.17
MgO	2.94	0.11	0.01	1.49	0.85	0.01	0.02	3.47	1.43	3.3	9.01	5.32	1.66	2.91	3.53	1.34	3.76	0.83	2.27	1.94	3.97	6.30	6.60	6.58	3.09	6.21	2.16	2.63	4.05	4.00	4.37	10.39
CaO	4.35	0.33	0.24	2.14	1.63	0.27	0.36	5.25	2.01	5.41	7.46	6.65	3.72	4.8	5.83	4.54	4.42	5.54	5.08	5.11	6.00	8.72	7.98	8.87	5.69	7.57	7.16	3.78	7.98	6.04	11.54	8.62
Na_2O	4.52	5.96	5.96	5.52	6.02	5.24	4.25	4.85	5.35	4.2	5.68	6.21	4.71	4.37	4.3	5.71	7.02	8.98	8.17	4.55	3.87	3.74	3.60	3.16	3.82	3.80	6.78	8.22	6.32	3.80	5.16	3.95
K_2O	2.51	6.14	7.63	5.59	5.59	4.26	4.76	3.13	4.19	3.45	0.49	1.26	3.86	3.07	2.42	4.57	1.27	0.57	0.11	2.62	2.71	1.85	1.75	2.01	2.80	2.12	0.25	0.41	0.61	2.60	0.35	0.40
P_2O_5	0.16	0.02	0.08	0.28	0.15	0.01	0.03	0.37	0.21	0.40	0.25	0.43	0.20	0.29	0.30	0.27	0.46	0.23	0.27	0.25	0.28	0.34	0.37	0.41	0.29	0.38	0.23	0.21	0.35	0.28	0.32	0.29
LOI	1.68	0.94	0.65	0.83	0.94	0.65	0.59	0.75	1.71	0.94	1.58	1.13	1.68	0.74	1.68	1.63	2.24	0	1.38	1.12	1.27	2.05	1.79	1.46	1.43	2.45	1.05	1.57	2.15	1.03	1.26	2.92
Total	100.2	99.60	99.35	99.69	99.43	99.33	99.43	99.68	99.81	99.80	100.4	99.8	99.35	99.91	100.0	99.54	100.2	100.0	100.3	99.39	99.81	100.2	100.4	99.97	99.88	100.1	99.62	100.3	99.72	99.61	99.90	100.3
Mg#	55	14	2	35	32	1	2	50	43	48	79	57	41	49	48	40	51	60	44	40	52	54	56	53	46	57	62	51	73	52	72	70
(ppm)																																
Rb	45	238	93	152	339	97	140	49	53	70	10	40	52	40	40	57	34	12	2	33	45	39	36	41	50	24	7	8	9	90	8	6
Sr	1,004	263	682	841	923	45	38	782	607	881	588	512	538	810	878	395	453	133	525	868	699	670	602	732	750	791	841	475	688	707	1290	569
Ba	1,120	240	752	722	728	136	64	739	994	826	139	480	1327	970	991	846	274	105	31	1,471	1,171	540	603	907	1185	685	340	173	271	1202	560	116
Zr	88	494	177	239	176	470	494	107	164	153	120	158	240	93	124	162	167	133	175	171	139	103	163	80	159	115	153	144	162	142	158	109
Hf	2.7	14.8	4.7	6.5	3.6	14.9	17.4	3.0	4.4	4.3	3.4	4.5	6.6	3.1	3.9	4.6	4.9	4.0	5.6	4.7	4.0	3.5	4.6	2.7	5.3	3.9	4.7	4.5	4.9	4.6	5.1	4.0
U	0.7	4.0	1.5	3.0	1.6	4.6	11.9	0.4	0.9	0.3	0.3	0.9	1.4	0.2	0.7	0.9	0.9	1.2	1.3	0.6	1.0	0.8	1.0	0.3	1.1	0.9	0.8	1.3	1.0	1.1	1.7	0.4
Th	2.2	17.4	3.2	9.4	7.2	7.8	27.0	2.4	3.4	3.1	3.4	3.1	4.4	2.9	2.0	3.6	5.7	5.0	4.3	2.4	4.0	4.1	3.8	1.4	4.5	3.9	3.1	4.9	3.3	4.5	5.8	3.0
Pb	13.5	10.1	14.6	6.3	16.6	8.9	5.9	5.4	6.4	7.1	1.0	3.8	3.0	6.6	10.2	7.0	0.4	0.6	0.6	7.2	6.6	4.4	4.0	4.2	9.1	2.9	2.9	1.0	0.8	7.1	2.4	2.7
Nb	3.4	30.4	7.5	10.9	9.7	5.7	8.2	4.3	4.5	6.6	6.2	7.7	7.0	6.0	6.0	6.5	7.7	5.2	7.5	5.5	6.7	6.5	7.8	3.9	8.6	6.5	6.8	7.3	8.5	7.9	7.5	7.6
V	78	27	41	89	83	137	74	87	66	87	124	207	95	63	134	81	162	48	62	61	157	273	235	239	154	223	104	119	147	168	148	210
Y	8.4	5.8	3.9	13.4	11.9	4.5	5.7	11.7	11.9	15.3	11.8	20.1	14.2	12.6	16.6	14.5	19.1	12.3	15.7	15.7	11.3	19.3	19.8	18.2	20.1	20.4	16.9	16.8	22.4	17.8	18.2	20.1
Cr	106.4	1.0	4.6	25.6	9.3	3.8	1.0	80.1	57.2	58.2	507.9	133.0	9.1	33.6	82.2	3.3	8.8	10.63	5.6	13.7	92.9	137.4	207.2	92.8	26.8	218.0	8.6	8.8	42.2	88.4	117.3	501.7
Co	11.8	0.4	0.6	10.0	5.5	0.5	2.3	10.9	7.7	14.1	23.6	30.8	9.8	13.7	18.1	3.4	7.2	1.1	4.3	11.2	22.3	34.4	33.4	31.8	19.6	37.2	5.7	11.8	10.1	24.7	13.0	42.0
Ni	35.5	5.3	3.8	12.7	6.6	4.9	4.1	22.5	16.6	16.5	164.1	29.8	6.1	26.6	26.4	6.8	8.3	4.4	5.7	9.9	27.3	24.1	61.1	25.6	8.0	55.1	8.0	6.5	13.3	24.3	21.1	222.4
Sc	8.1	0.7	0.3	5.6	1.9	1.0	0.1	5.9	6.3	10.3	14.4	21.0	8.0	7.5	9.4	6.5	9.2	1.6	5.5	5.4	7.5	17.9	23.8	23.1	17.2	25.8	8.7	5.2	14.9	18.6	17.3	26.8
La	14.69	21.56	9.95	28.97	24.24	4.96	8.78	24.51	18.87	26.99	12.35	26.58	34.51	32.09	28.16	30.8	27.44	15.1	24.05	31.98	29.08	22.98	29.71	18.81	32.02	29.03	29.39	26.42	33.22	32.35	35.76	24.05
Ce	27.50	48.69	17.74	56.08	52.77	8.93	14.74	49.56	32.71	57.57	28.49	55.85	64.43	66.97	56.69	60.63	58.69	38.99	56.78	65.43	54.16	48.9	64.18	43.04	62.88	60.85	60.13	55.54	67.17	61.99	69.05	56.11
Pr	3.04	4.12	1.88	5.74	4.62	0.80	1.25	5.82	4.14	6.43	3.64	6.68	6.97	7.16	6.69	6.80	7.02	4.20	5.60	6.91	5.98	6.04	7.38	5.03	7.31	7.15	6.28	6.21	7.87	6.66	7.44	6.74
Nd	12.38	15.45	7.26	23.77	17.45	3.66	6.38	24.92	17.58	29.03	16.69	25.95	28.31	29.46	28.33	28.71	32.39	18.33	25.8	30.35	24.66	28.49	33.15	24.95	31.87	33.77	28.01	21.14	33.98	29.04	32.51	31.08
Sm	2.26	3.01	1.23	4.41	3.33	0.62	0.92	4.58	3.22	5.24	3.48	5.21	4.68	4.90	5.31	4.99	6.24	3.69	4.52	5.40	4.50	5.82	6.56	4.92	5.53	6.31	4.78	3.75	5.89	5.21	5.73	5.78
Eu	0.89	0.98	0.47	1.37	1.04	0.19	0.23	1.37	1.28	1.67	1.10	1.96	1.57	1.55	1.80	1.48	1.71	1.18	1.51	1.86	1.54	1.83	1.96	1.96	2.12	2.22	1.83	1.64	2.12	1.93	2.07	2.03
Gd	2.08	2.56	1.07	3.78	2.86	0.52	0.61	3.64	2.79	4.67	3.04	4.62	3.65	4.10	4.47	4.22	5.31	3.19	3.78	4.49	3.74	5.18	5.22	4.45	4.72	5.26	3.92	3.54	5.27	4.08	4.63	4.69
Tb	0.28	0.35	0.14	0.55	0.39	0.08	0.10	0.50	0.39	0.62	0.41	0.59	0.49	0.52	0.61	0.58	0.75	0.45	0.54	0.61	0.50	0.71	0.73	0.62	0.65	0.72	0.55	0.52	0.71	0.57	0.63	0.64
Dy	1.61	1.91	0.79	2.98	2.02	0.55	0.72	2.68	2.18	3.47	2.31	3.09	2.60	2.80	3.32	2.98	3.88	2.51	2.96	3.47	2.73	4.05	3.80	3.58	3.75	3.94	3.20	3.09	4.02	3.32	3.58	3.89
Ho	0.32	0.36	0.15	0.57	0.38	0.13	0.17	0.51	0.43	0.66	0.45	0.59	0.54	0.54	0.64	0.58	0.79	0.50	0.55	0.67	0.53	0.78	0.80	0.69	0.73	0.74	0.62	0.59	0.79	0.62	0.68	0.71
Er	0.92	1.11	0.52	1.67	1.16	0.51	0.65	1.53	1.36	1.85	1.31	1.58	1.61	1.48	1.87	1.66	2.20	1.54	1.58	2.01	1.53	2.28	2.29	1.84	2.03	2.07	1.73	1.73	2.15	1.82	1.85	2.05
Tm	0.14	0.15	0.08	0.25	0.16	0.10	0.15	0.21	0.20	0.27	0.19	0.24	0.25	0.21	0.26	0.25	0.31	0.23	0.24	0.30	0.23	0.32	0.33	0.26	0.31	0.30	0.27	0.27	0.31	0.26	0.28	0.30
Yb	0.96	1.12	0.58	1.62	1.20	1.08	1.28	1.38	1.46	1.73	1.23	1.62	1.77	1.39	1.82	1.62	2.08	1.49	1.55	1.90	1.48	2.03	2.20	1.47	1.95	1.89	1.79	1.82	2.10	1.69	1.84	1.93
Lu	0.15	0.17	0.08	0.25	0.18	0.20	0.22	0.21	0.24	0.27	0.19	0.25	0.30	0.21	0.28	0.25	0.31	0.22	0.25	0.31	0.22	0.31	0.34	0.22	0.31	0.28	0.29	0.29	0.31	0.26	0.28	0.29
Eu/Eu*	1.27	1.09	1.27	1.04	1.04	1.04	0.95	1.04	1.32	1.05	1.05	1.24	1.18	1.07	1.14	1.00	0.92	1.07	1.13	1.17	1.16	1.03	1.04	1.30	1.28	1.19	1.31	1.39	1.18	1.30	1.24	1.21

Note: *syen* syenite, *gran* granite, *mz* monzonite, *q.mz* quartz monzonite, *dio* diorite, *mz.di* monzodiorite, *gbb* gabbro, Samples: *HS* Hongshan suite, *QC, SDC, HL, PH* Wu'an suite, *XS* Xishu suite, Mg# = 100×molar Mg/(Mg + 0.9×Fe)

Table 2 Rb–Sr and Sm–Nd isotope compositions for rocks from southern Taihang, North China

Sample No.	[Rb] ppm	[Sr] ppm	$^{87}Rb/^{86}Sr$	$^{87}Sr/^{86}Sr$	2σm	I_{Sr} 135 Ma	[Sm] ppm	[Nd] ppm	$^{147}Sm/^{144}Nd$	$^{143}Nd/^{144}Nd$	2σm	$\varepsilon_{Nd}(0)$	$\varepsilon_{Nd}(T)$ 135 Ma	f Sm/Nd	T_{DM} (Ga)
HS-1	46.50	1006.0	0.1336	0.705799	20	0.70554	2.480	12.76	0.1175	0.511998	10	−12.5	−11.1	−0.40	1.82
HS-2[a]	232.8	260.4	2.5843	0.711976	6	0.70702	3.025	17.08	0.1071	0.512010	3	−12.3	−10.7	−0.46	1.63
HS-8	94.00	697.4	0.3899	0.708094	19	0.70735	1.473	8.692	0.1025	0.512081	11	−10.9	−9.2	−0.48	1.46
HS-14	159.8	875.8	0.5280	0.707131	18	0.70612	4.268	21.17	0.1219	0.512087	11	−10.7	−9.5	−0.38	1.76
HS-17	342.2	948.0	1.0442	0.707170	19	0.70517	2.810	15.11	0.1125	0.512141	10	−9.7	−8.2	−0.43	1.52
HS-11	106.5	51.86	5.9460	0.717570	32	0.70616	0.641	3.662	0.1059	0.512135	11	−9.8	−8.2	−0.46	1.43
HS-12	140.5	39.04	10.433	0.730190	50	0.71017	0.946	6.505	0.0879	0.512057	11	−11.3	−9.5	−0.55	1.32
QC-1[a]	52.93	790.5	0.1934	0.707688	6	0.70732	5.203	28.39	0.1108	0.511644	3	−19.4	−17.9	−0.44	2.22
QC-1	52.40	791.1	0.1914	0.707899	15	0.70753	5.153	27.45	0.1135	0.511674	9	−18.8	−17.4	−0.42	2.24
QC-3	63.70	603.1	0.3057	0.707437	13	0.70685	2.766	14.58	0.1147	0.511747	14	−17.4	−16.0	−0.42	2.15
QC-5	69.60	888.6	0.2267	0.708054	18	0.70762	4.962	24.94	0.1203	0.511640	10	−19.5	−18.2	−0.39	2.45
QC-6	12.10	626.8	0.0558	0.707340	20	0.70723	3.140	14.84	0.1280	0.511783	14	−16.7	−15.5	−0.35	2.42
QC-7	25.94	742.3	0.1015	0.706625	18	0.70643	4.950	24.81	0.1206	0.511768	10	−17.0	−15.7	−0.39	2.25
SDC-2[a]	58.04	550.6	0.3045	0.706606	7	0.70602	4.037	24.39	0.1001	0.511727	4	−17.8	−16.1	−0.49	1.90
SDC-2	58.10	543.9	0.3089	0.706568	15	0.70598	4.246	24.69	0.1040	0.511728	10	−17.8	−16.2	−0.47	1.97
SDC-3[a]	43.67	828.2	0.1523	0.706411	7	0.70612	4.769	27.71	0.1040	0.511665	4	−19.0	−17.4	−0.47	2.06
SDC-3	42.80	833.4	0.1487	0.706588	15	0.70630	4.490	24.67	0.1101	0.511683	12	−18.6	−17.1	−0.44	2.15
SDC-4[a]	40.09	901.0	0.1285	0.706123	7	0.70588	4.658	25.08	0.1123	0.511708	3	−18.1	−16.7	−0.43	2.16
SDC-4	40.94	909.9	0.1302	0.706094	13	0.70584	4.279	22.55	0.1148	0.511777	20	−16.8	−15.4	−0.42	2.11
HL-1	63.30	403.5	0.4537	0.708402	20	0.70753	5.103	27.31	0.1130	0.511715	9	−18.0	−16.6	−0.43	2.16
HL-6[a]	33.44	487.9	0.1980	0.706782	7	0.70640	5.733	29.51	0.1174	0.511664	4	−19.0	−17.6	−0.40	2.34
HL-6	35.10	498.7	0.2036	0.706891	18	0.70650	5.059	24.85	0.1231	0.511683	9	−18.6	−17.4	−0.37	2.46
HL-7	13.10	145.7	0.2602	0.707811	14	0.70731	3.610	18.17	0.1202	0.511861	12	−15.2	−13.8	−0.39	2.09
HL-10	2.40	529.4	0.0130	0.707131	20	0.70711	4.270	23.28	0.1109	0.511673	11	−18.8	−17.3	−0.44	2.18
PH-1[a]	35.83	871.0	0.1188	0.706664	6	0.70644	5.087	28.05	0.1096	0.511713	3	−18.0	−16.5	−0.44	2.10
PH-1	40.10	884.4	0.1312	0.706851	18	0.70660	5.089	25.96	0.1186	0.511723	15	−17.8	−16.5	−0.40	2.28
XS-1[a]	45.24	745.7	0.1752	0.706426	7	0.70609	4.236	23.40	0.1094	0.511831	3	−15.7	−14.2	−0.44	1.92
XS-1	47.10	747.6	0.1822	0.706655	14	0.70631	4.420	23.91	0.1124	0.511853	10	−15.3	−13.9	−0.43	1.95
XS-2[a]	38.17	717.8	0.1536	0.706391	6	0.70610	5.213	25.36	0.1242	0.511813	3	−16.1	−14.8	−0.37	2.27
XS-2	40.20	726.4	0.1599	0.706401	14	0.70609	4.916	23.57	0.1261	0.511851	9	−15.4	−14.1	−0.36	2.25
XS-3[a]	36.04	672.3	0.1549	0.706882	6	0.70658	5.703	29.79	0.1157	0.511852	3	−15.3	−13.9	−0.41	2.01
XS-3	39.30	719.1	0.1577	0.706847	20	0.70654	6.455	32.53	0.1200	0.511863	11	−15.1	−13.8	−0.39	2.09
XS-4[a]	41.21	749.7	0.1588	0.706329	7	0.70602	5.081	24.65	0.1246	0.511819	3	−16.0	−14.7	−0.37	2.27
XS-4	41.00	769.0	0.1543	0.706325	15	0.70603	5.507	26.14	0.1274	0.511866	12	−15.1	−13.9	−0.35	2.26
XS-8	49.90	749.7	0.1927	0.706444	20	0.70607	5.032	27.26	0.1116	0.511791	11	−16.5	−15.1	−0.43	2.02
XS-10[a]	24.93	748.9	0.0961	0.706264	8	0.70608	5.431	27.95	0.1174	0.511880	3	−14.8	−13.4	−0.40	2.00
XS-10	27.60	779.6	0.1025	0.706260	20	0.70606	5.662	28.83	0.1188	0.511895	10	−14.5	−13.2	−0.40	2.01
XS-11	7.42	820.2	0.0262	0.706143	15	0.70609	4.096	22.47	0.1102	0.511695	10	−18.4	−16.9	−0.44	2.13
XS-12	8.61	473.0	0.0526	0.707236	18	0.70714	3.707	19.65	0.1141	0.511912	10	−14.2	−12.7	−0.42	1.89
XS-13	9.80	690.8	0.0410	0.707750	18	0.70767	5.569	29.66	0.1136	0.511731	7	−17.7	−16.3	−0.42	2.15
XS-15	92.10	713.6	0.3732	0.706297	20	0.70558	4.420	24.12	0.1109	0.511865	10	−15.1	−13.6	−0.44	1.90
XS-20	8.80	1240.1	0.0206	0.706730	13	0.70669	5.106	27.54	0.1121	0.511935	13	−13.7	−12.3	−0.43	1.82
XS-24	6.84	584.9	0.0338	0.706112	22	0.70605	6.042	30.61	0.1194	0.511865	7	−15.1	−13.7	−0.39	2.07

Note: $\varepsilon_{Nd} = \left(\left(^{143}Nd/^{144}Nd\right)_s/\left(^{143}Nd/^{144}Nd\right)_{CHUR} - 1\right) \times 10{,}000$, $f_{Sm/Nd} = \left(^{147}Sm/^{144}Nd\right)_s/\left(^{147}Sm/^{144}Nd\right)_{CHUR} - 1$, where s = sample, $\left(^{143}Nd/^{144}Nd\right)_{CHUR} = 0.512638$ and $\left(^{147}Sm/^{144}Nd\right)_{CHUR} = 0.1967$. Model age ($T_{DM}$) is calculated using a linear isotopic ratio growth equation: $T_{DM} = 1/\lambda \times \ln\left(1 + \left(\left(^{143}Nd/^{144}Nd\right)_s - 0.51315\right)/\left(\left(^{147}Sm/^{144}Nd\right)_s - 0.2137\right)\right)$. [a]Samples analyzed in Rennes, and the remainders in Beijing

Table 3 Lead isotopic analyses for magmatic rocks from southern Taihang, North China

Sample No.	$^{206}Pb/^{204}Pb$	$^{207}Pb/^{204}Pb$	$^{208}Pb/^{204}Pb$	$^{238}U/^{204}Pb$	$^{235}U/^{204}Pb$	$^{232}Th/^{204}Pb$	$(^{206}Pb/^{204}Pb)_i$	$(^{207}Pb/^{204}Pb)_i$	$(^{208}Pb/^{204}Pb)_i$	Δ7/4	Δ8/4
HS-1	17.352	15.378	37.284	2.993	0.0216	10.265	17.288	15.375	37.216	1.0	68.7
HS-2	18.217	15.462	38.569	24.453	0.1766	110.020	17.700	15.437	37.832	2.8	80.6
HS-8	16.336	14.098	34.610	6.371	0.0460	14.299	16.201	14.092	34.514	−115.0	−70.0
HS-14	18.399	15.477	38.328	29.080	0.2100	95.941	17.783	15.447	37.685	2.9	55.8
HS-17	17.676	15.427	37.756	5.855	0.0423	28.005	17.552	15.421	37.568	2.7	72.0
HS-11	18.043	15.434	37.787	91.456	0.6606	110.715	17.370	15.401	37.414	2.7	78.7
HS-12	20.406	15.530	40.062	103.833	0.7500	510.791	17.514	15.390	38.084	0.0	128.2
QC-1	16.768	15.287	36.975	4.400	0.0318	28.804	16.675	15.283	36.782	−1.6	99.5
QC-3	17.085	15.343	37.218	8.345	0.0603	33.752	16.908	15.334	36.992	1.0	92.2
QC-5	16.775	15.304	36.996	2.892	0.0209	27.764	16.714	15.301	36.810	−0.1	97.6
QC-6	17.472	15.386	38.501	17.971	0.1298	211.448	17.091	15.368	37.084	2.4	79.4
SDC-2	17.512	15.463	37.755	27.666	0.1998	92.854	16.927	15.435	37.133	10.9	104.2
SDC-3	16.863	15.306	37.022	1.412	0.0102	27.876	16.834	15.304	36.835	−1.2	85.6
SDC-4	16.974	15.321	36.928	4.096	0.0296	12.873	16.887	15.317	36.841	−0.5	79.8
HL-1	17.360	15.377	37.567	8.064	0.0583	32.470	17.189	15.368	37.349	1.4	94.1
HL-6	19.516	15.438	42.546	13.619	0.0984	56.823	16.634	15.298	36.834	0.4	109.7
HL-7	19.973	15.523	41.187	60.593	0.4377	261.604	17.048	15.382	37.285	4.3	104.7
HL-10	20.197	15.569	40.992	127.615	0.9218	442.840	17.496	15.438	38.024	5.0	124.4
PH-1	16.965	15.330	36.899	4.752	0.0343	21.582	16.865	15.325	36.755	0.6	73.8
XS-1	17.360	15.379	37.693	9.388	0.0678	38.952	17.162	15.369	37.432	1.8	105.7
XS-2	17.493	15.420	37.895	11.867	0.0857	59.197	17.242	15.408	37.499	4.8	102.6
XS-3	17.545	15.401	37.814	15.536	0.1122	61.547	17.216	15.385	37.401	2.8	96.0
XS-4	17.177	15.323	37.306	3.857	0.0279	21.127	17.095	15.319	37.164	−2.5	87.0
XS-8	17.090	15.352	37.371	7.848	0.0567	32.114	16.924	15.344	37.156	1.8	106.8
XS-10	17.671	15.418	38.069	19.252	0.1391	85.957	17.264	15.398	37.493	3.6	99.4
XS-11	17.413	15.384	37.701	18.362	0.1326	70.166	17.024	15.365	37.230	2.9	102.1
XS-12	19.025	15.507	39.737	97.158	0.7018	374.318	17.298	15.423	37.630	5.7	109.0
XS-13	18.797	15.454	39.272	120.786	0.8724	433.041	17.231	15.378	37.494	1.9	103.4
XS-15	17.277	15.347	37.536	9.477	0.0685	40.754	17.076	15.337	37.263	−0.5	99.1
XS-20	17.951	15.391	38.408	43.429	0.3137	155.547	17.032	15.346	37.366	0.9	114.8
XS-24	17.340	15.360	37.755	9.777	0.0706	71.105	17.133	15.350	37.278	0.2	93.7

Note: Initial Pb isotope ratios were calculated by assuming $t = 135$ Ma. $\Delta 7/4 = \left(\left(^{207}Pb/^{204}Pb\right)_i - \left(^{207}Pb/^{204}Pb\right)_{NHRL}\right) \times 100$; $\Delta 8/4 = \left(\left(^{208}Pb/^{204}Pb\right)_i - \left(^{208}Pb/^{204}Pb\right)_{NHRL}\right) \times 100$; $\left(^{207}Pb/^{204}Pb\right)_{NHRL} = 0.1084 \times \left(^{206}Pb/^{204}Pb\right)_i + 13.491$, $\left(^{208}Pb/^{204}Pb\right)_{NHRL} = 1.209 \times \left(^{206}Pb/^{204}Pb\right)_i + 15.627$ (Hart 1984)

spectrometer at the IGG (Beijing). Repeated analyses of NBS981 yielded $^{204}Pb/^{206}Pb = 0.05897 \pm 15$, $^{207}Pb/^{206}Pb = 0.91445 \pm 80$, and $^{208}Pb/^{206}Pb = 2.16170 \pm 200$. The Pb isotopic data are presented in Table 3.

Results

Major and trace elements

As shown in a classification diagram $K_2O + Na_2O$ versus SiO_2 (Fig. 2; Middlemost 1994), the Xishu suite is dominated by gabbroic diorite and monzonite, Wu'an suite by monzonite and quartz monzonite, and Hongshan suite by syenite–granite. The Xishu and Wu'an suites show large variations in chemical compositions (Fig. 3), but the former (with $SiO_2 = 50$–61%, $Mg\# = 73$–46) are slightly less differentiated than the latter (with $SiO_2 = 54$–64%, $Mg\# = 79$–40; Table 1). Both Xishu and Wu'an rocks are alkali-rich with $Na_2O > K_2O$. The Wu'an rocks show similar variation trends to the Xishu rocks in most Harker plots (Fig. 3). This could be interpreted as reflecting a genetic link between the two. Except for P_2O_5 that shows a convex curve, CaO, MgO, FeO and TiO_2 are negatively linearly correlated with SiO_2, but Al_2O_3 positively correlated (Fig. 3). This indicates a significant fractionation of ferromagnesian phases during magma evolution. However, XS-20 is exceptionally CaO-rich (11.54%; Fig. 3). This could reflect a plagioclase cumulate character, which is consistent with its high Sr (1,240 ppm; Fig. 4) and high modal proportion of plagioclase. Similarly, QC-6 and XS-24 deviate from the evolution trends in plots of SiO_2 vs. MgO and Al_2O_3 by lower Al_2O_3 and higher MgO when compared with samples with similar SiO_2 contents (Fig. 3). This is likely attributed to hornblende and Cpx cumulate in the two, as is supported by the very high Cr abundances (508 ppm for QC-6 and 502 ppm for XS-24; Table 1) and relatively high CaO (7.46 and 8.62%; Table 1) as well as our petrographical observations (main rock-forming minerals for QC-6 are hornblende 35% + Cpx 25% + plagioclase 27% + quartz 10%, and for XS-24 hornblende 30% + Cpx 38% + biotite 5% + plagioclase 20% + quartz 3%). The co-magmatic nature of the Xishu and Wuan rocks can also be seen from the plots of trace elements vs. SiO_2 (Fig. 4), where they exhibit regular variations with increasing SiO_2, approximately linear

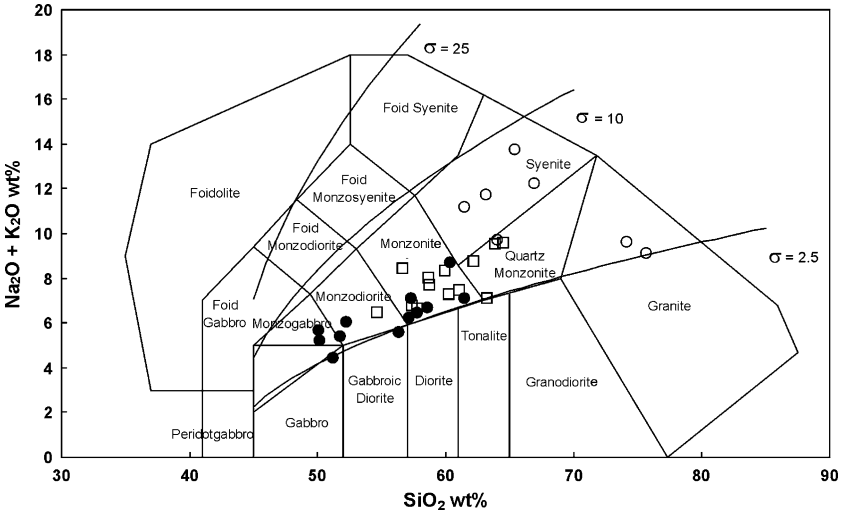

Fig. 2 Classification diagram (Middlemost 1994) for the Xishu (*filled circle*), Wu'an (*open square*) and Hongshan (*open circle*) suites

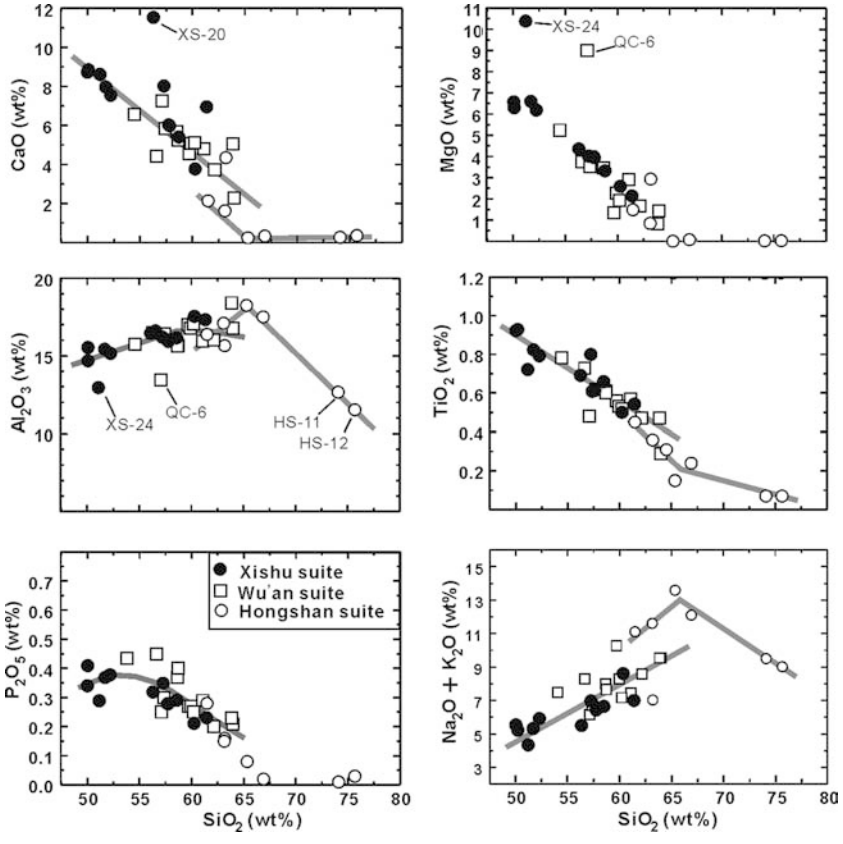

Fig. 3 Harker diagrams for the Xishu (*filled circle*), Wu'an (*open square*) and Hongshan (*open circle*) suites

(U, Th, Sc, Co, and V), or curvilinear (Zr and Y), but showing scattering in Sr and Rb. All rock types of the Xishu and Wu'an suites show rather similar REE patterns (Fig. 5a, b), with highly enriched LREE and positive- to minor Eu anomalies ($Eu/Eu^* = 1.39–0.92$; Table 1). In the primitive mantle-normalized spidergrams (Fig. 5d, e), they are characterized by spikes in LILEs (e.g., Sr, Ba, Th, K) and LREE, and troughs in HFSEs (e.g., Nb and Ti).

The Hongshan syenites also exhibit a significant variation in chemical compositions, with $SiO_2 = 61–67\%$ (Table 1). Most of them have high K_2O (5.5–7.6%) and Na_2O (5.5–6.0%). Granites (HS-11 and HS-12) differ from syenites by higher SiO_2 (>74%) and lower Al_2O_3 (11.5–12.6%) and alkalis (Fig. 3). A striking feature is that the Hongshan syenites–granites plot in different fields and show variation trends independent of the Xishu–Wu'an complexes. This is particularly true in plots CaO, Al_2O_3, TiO_2 and alkalis (Fig. 3) and U, Th, Sr, Rb and Zr (Fig. 4). All syenites REE patterns are LREE-enriched, with minor to positive Eu anomalies and highly depleted HREE (Fig. 5c) and Y (Fig. 4),

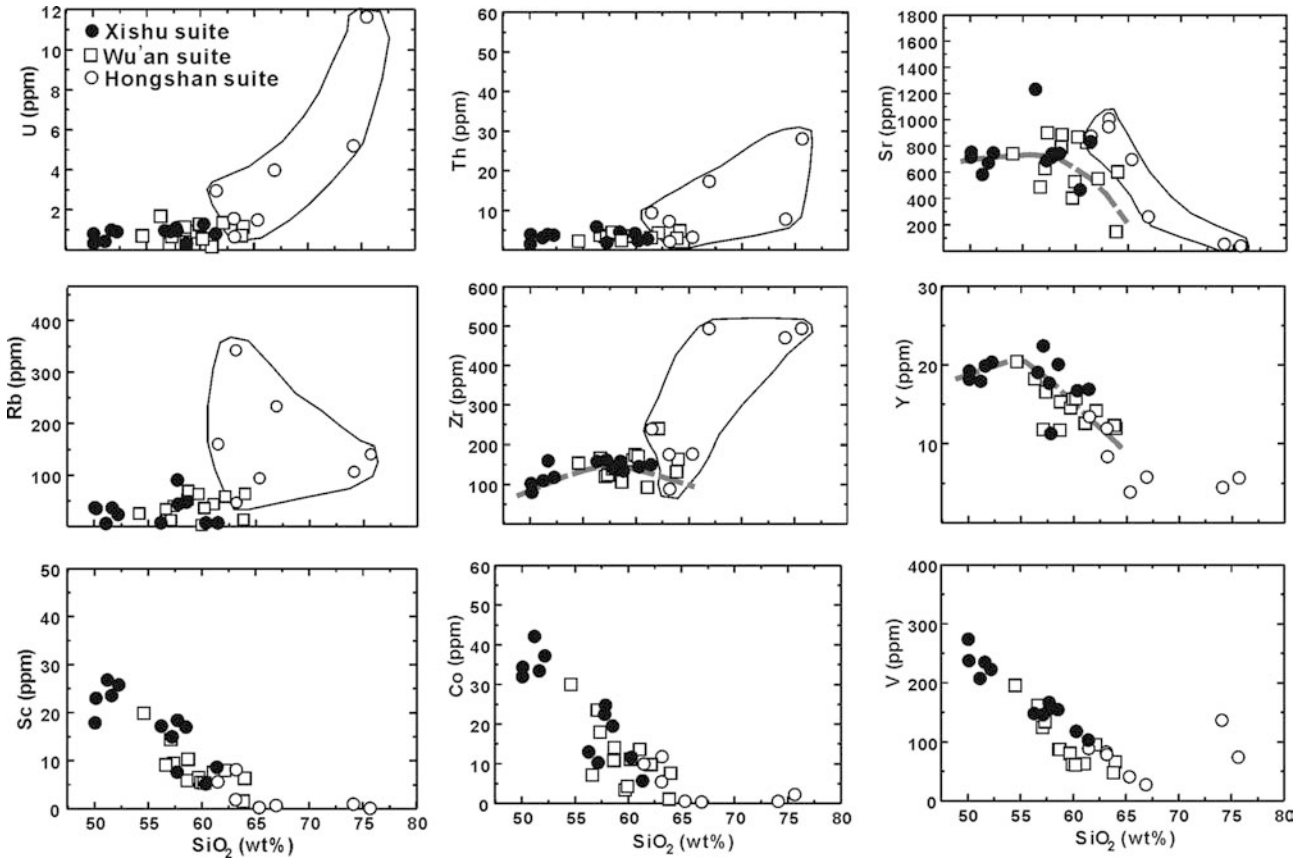

Fig. 4 Plots of selected trace elements vs. silica for the Xishu (*filled circle*), Wu'an (*open square*) and Hongshan (*open circle*) suites. Note that Hongshan syenite–granites plot in different fields from the Xishu–Wu'an monzonitic rocks

implying an important role of residual garnet in the source. The two granites, however, show remarkable middle REE depletion and negligible Eu anomalies, with concave-shaped REE patterns (Fig. 5c). In the spidergrams (Fig. 5f), Hongshan rocks display positive anomalies of Rb, Th, K, Sr, Zr and LREE, and negative anomalies of Ba, Ti and Nb.

Sr–Nd–Pb isotopes

Most Xishu rocks have moderately high initial $^{87}Sr/^{86}Sr$ ratios (I_{Sr}) ranging from 0.7056 to 0.7071, and low ε_{Nd}(135 Ma) values from −12.3 to −16.9. However, their data rather scatter in a plot I_{Sr} vs. ε_{Nd}(135 Ma) (Fig. 6a). The Wu'an monzonitic rocks have I_{Sr} from 0.7059 to 0.7076 and ε_{Nd}(135 Ma) from −13.8 to −18. The fields for the two suites cannot be completely separated, but they show some difference (Fig. 6a). By contrast, the Hongshan syenites–granites differ from Xishu–Wu'an monzonitic rocks by obviously higher ε_{Nd}(135 Ma) values (from −8.2 to −11), and rather varied I_{Sr} (from 0.7052 to 0.7102), and roughly a flat trend can be seen for the syenite–granite suite (Fig. 6a). The very high I_{Sr} of HS-12 (0.7102) is only a face value; its high $^{87}Rb/^{86}Sr$ ratio (10.4) would produce a large uncertainty in the calculated I_{Sr} (Jahn et al. 2000).

Lead isotopic ratios of the three suites are shown in Fig. 6b, c. ^{208}Pb data are slightly more radiogenic than ^{206}Pb, so that these rocks plot to the left of the north hemisphere reference line (NHRL). Also plotted for comparison are EM1 (enriched mantle with intermediate $^{87}Sr/^{86}Sr$, low $^{143}Nd/^{144}Nd$ and low $^{206}Pb/^{204}Pb$), EM2 (enriched mantle with high $^{87}Sr/^{86}Sr$, high $^{206}Pb/^{204}Pb$, and intermediate $^{143}Nd/^{144}Nd$; Zindler and Hart 1986) and LCC (lower continental crust of the NCC with low Pb isotopic ratios $^{206}Pb/^{204}Pb = 14–17.5$, $^{207}Pb/^{204}Pb = 14.6–15.4$, $^{208}Pb/^{204}Pb = 34.3–36.5$; Zhu 1991). Lead isotopic data of the Mesozoic Fangcheng basalts (within the NCC; Zhang et al. 2002) were shown for reference, which were thought to reflect the Pb isotopic signature of the enriched mantle beneath NCC. All three rock suites plot between the fields of the EM1 and of LCC, suggesting a mixing process between LCC and EM1 components for their genesis. Xishu and Wu'an rocks form continuous variation trends in the Pb isotopic ratio plots, with the Xishu rocks ($(^{206}Pb/^{204}Pb)_i = 16.92–17.3$, $^{207}Pb/^{204}Pb = 15.32–15.42$, $^{208}Pb/^{204}Pb = 37.16–37.63$) having faintly higher Pb isotopic ratios than the Wu'an rocks (mostly 16.63–17.4, 15.28–15.44, 36.78–37.3, respectively). Hongshan syenites–granites show Pb isotopic ratios higher than Xishu–Wu'an rocks (Fig. 6b, c), plotting close to the EM1 field. But sample HS-8 has very low Pb isotope ratios (Fig. 6c), and the reason is unclear.

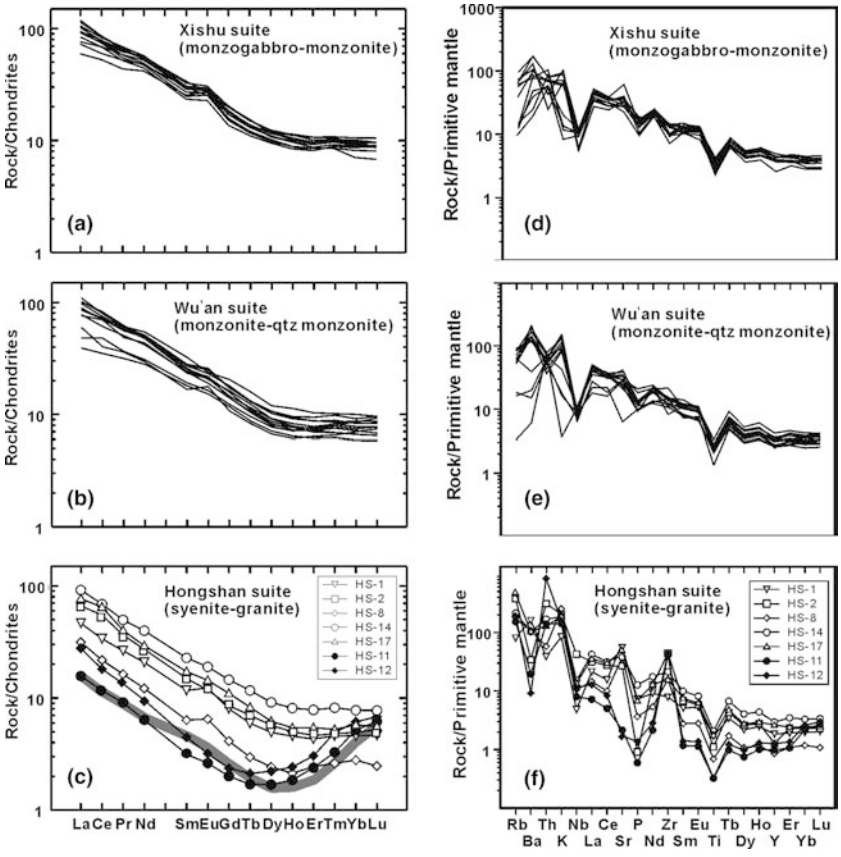

Fig. 5 Chondrites-normalized REE patterns and primitive mantle-normalized spidergrams for the Xishu, Wu'an and Hongshan suites. Chondrite values are from Masuda et al. (1973), further divided by 1.2; primitive mantle values from Sun and McDonough (1989). The *grey curve* in (c) represents calculated pattern for the residual melt after 22% hornblende–feldspar dominated fractionation (plus minor apaptite and allanite) from a syenitic parent (HS-14) based on the Rayleigh fractionation law. REE distribution coefficients for hornblende and apatite are from Arth (1976), feldspar from Nash and Crecraft (1985), and allanite from Brooks et al. (1981). Calculated bulk distribution coefficients are: La = 8.33, Ce = 8.41, Nd = 8.30, Sm = 7.33, Eu = 7.32, Gd = 7.54, Dy = 8.08, Er = 6.86, Yb = 3.56 and Lu = 2.48

Discussion

Petrogenesis of the Xishu–Wu'an monzonitic rocks

The Xishu rocks are characterized by comparatively low SiO_2 (mostly $< 58\%$) and high Mg# (mostly > 50). Theoretically, these rocks could originate from partial melting of a basic lower crust, or of a mantle source. However, recent experimental data (Rapp and Watson 1995; Wolf and Wyllie 1994) have shown that extremely high temperatures (~1,100°C) are required to produce metaluminous low-silica ($< 58\%$) melts by dehydration melting of metabasalts in the lower crust. Regardless of the degree of partial melting, such melts are generally characterized by low Mg# (< 42), which is not the case for Xishu rocks. Therefore, Xishu rocks cannot be generated by melting of basic lower crustal rocks, and a mantle source is required. This conclusion is supported by the occasional occurrence of peridotite xenoliths within the complex (Xu and Lin 1991).

The Wu'an monzonitic rocks are slightly more evolved than the Xishu rocks, but are also characterized by relatively low silica contents (54–64%, mostly $< 60\%$) and elevated Mg# (79–40). Consequently, they are unlikely pure crustal melts and a considerable amount of mantle-derived magma is required in their genesis. In fact, the co-magmatic nature of the Wu'an and Xishu rocks is readily suggested by the close temporal and spatial relationship of the two and the chemical trends shown in Figs. 3 and 4, as well as their similar REE patterns and spidergrams (Fig. 5). Therefore, the Wu'an rocks could originate from the Xishu rocks through coupled fractionation of ferromagnesian phases and assimilation of lower crustal components (= AFC process). This model is further verified in Fig. 7 where the two suites are closely associated as shown by the linear variation trends in I_{Sr} vs. 1/Sr (Fig. 7a), ε_{Nd}(135 Ma) vs. 1/Nd (Fig. 7b) and Rb/Sr vs. Rb (Fig. 7c). However, another possibility cannot be precluded that the Xishu and Wu'an suites were formed corresponding to different batch of melting of the same mantle source, with the internal differentiation by AFC more developed in the latter, as suggested by Xu and Lin (1991).

The sharp depletion of CaO, MgO, FeO and TiO_2 with increasing SiO_2 (Fig. 3) indicates a significant fractionation of ferromagnesian phases like pyroxene and hornblende during magma evolution, which is also supported by the negative correlation of SiO_2 with Sc, Co and V (Fig. 4). Separation of feldspar in Xishu rocks appears minor, as suggested by a positive correlation between Al_2O_3 and SiO_2 (Fig. 3) and positive Eu anomalies (Fig. 5a). However, it is complicated for Wu'an rocks with respect to feldspar removal, as revealed by the highly varied Eu/Eu* ratios ranging from 0.92 to 1.32 (Table 1), and the kinks in plots SiO_2 vs.

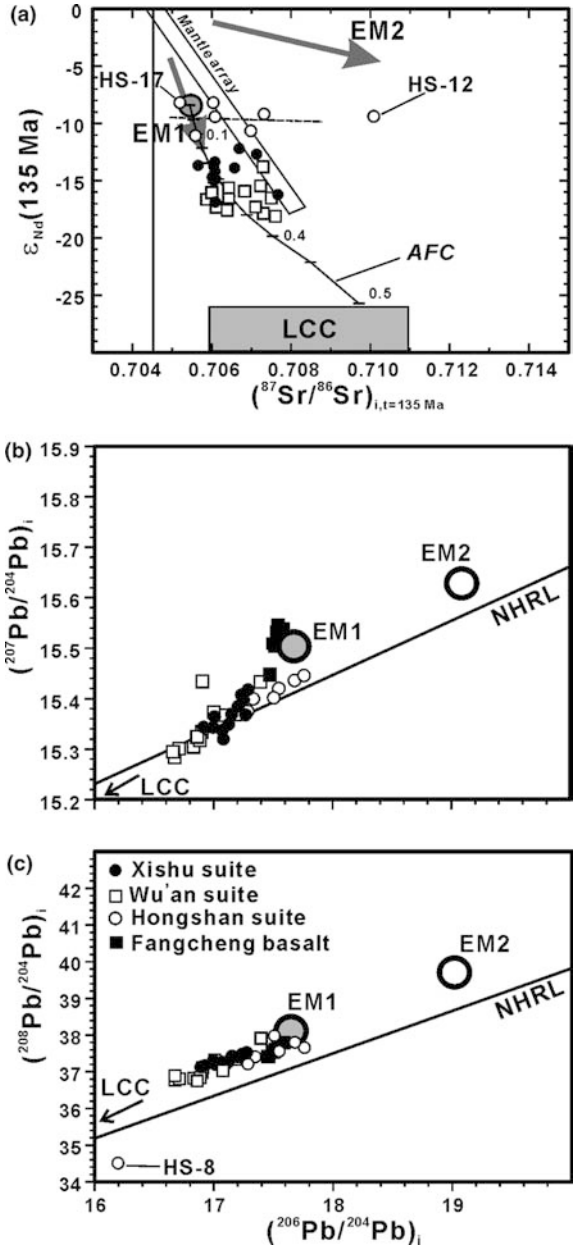

Fig. 6 **a** Plot of ε_{Nd}(135 Ma) vs. I_{Sr} ratios. Two end members assumed for the isotopic modeling based on an AFC model (DePaolo 1981) are the EM1-type mantle ($I_{Sr}=0.7055$, Sr = 1,100 ppm, $\varepsilon_{Nd}=-8.5$, Nd = 24 ppm; Chen et al. 2003; Chen and Zhai 2003) and LCC ($I_{Sr}=0.710$, Sr = 350 ppm, $\varepsilon_{Nd}=-30$, Nd = 26 ppm; Jahn et al. 1988); other parameters are $D_{Nd}=0.9$, $D_{Sr}=1.4$, $r=0.34$. The *dashed line* represents a roughly lateral variation trend for the Hongshan suite. **b** Plot of $^{207}Pb/^{204}Pb$ vs. $^{206}Pb/^{204}Pb$. **c** Plot of $^{208}Pb/^{204}Pb$ vs. $^{206}Pb/^{204}Pb$. The Mesozoic Fangcheng basalts (Zhang et al. 2002) were plotted for reference. *NHRL* north hemisphere reference line. Location of EM1 and EM2 is from Zindler and Hart (1986)

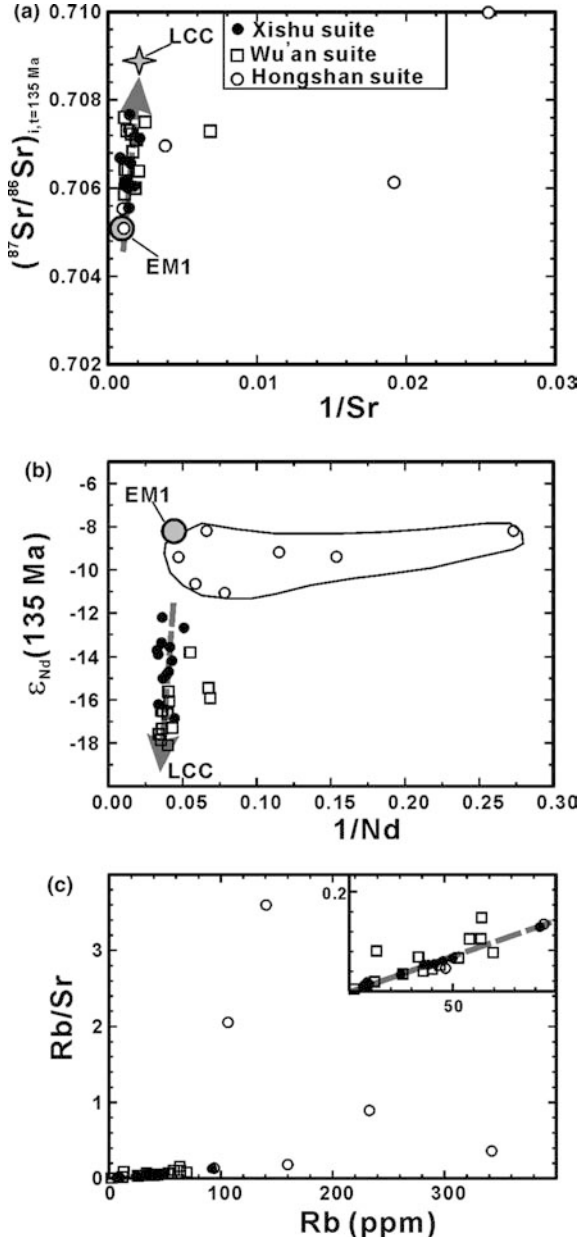

Fig. 7 Plots of **a** I_{Sr} vs. 1/Sr, **b** ε_{Nd}(135 Ma) vs. 1/Nd, and **c** Rb/Sr vs. Rb for the Xishu, Wu'an and Hongshan suites, showing the Xishu and Wu'an rocks are co-magmatic, plotting on the extension from EM1 (Chen and Zhai 2003; Chen et al. 2003) to LCC (Jahn et al. 1988) and Hongshan syenites–granites derived from a separate magma chamber

Al_2O_3 (Fig. 3) and SiO_2 vs. Sr (Fig. 4). The above argument suggests that feldspar removal is minor in an earlier stage, but significant in a later stage of magma evolution. Fractionation of accessory phases like zircon is important only in evolved rock types as is shown by the decreasing Zr and Y with increasing SiO_2 (Fig. 4).

On the other hand, our isotopic data indicate that Xishu–Wu'an rocks were not simply produced via fractionation of mantle-derived magmas in a closed system. The least differentiated members (SiO_2 = 50–52%) of the Xishu suite have high Sr concentrations (570–790 ppm), highly enriched LREE patterns (Fig. 5a) and distinctive Sr-Nd isotopic signatures ($I_{Sr}=0.706$–0.7066, ε_{Nd}(135 Ma) = −13 to −15). These features point to a long-term enriched SCLM source. Previous work on Mesozoic lamprophyres (Chen and Zhai 2003) and gabbros (Chen et al. 2003) revealed that

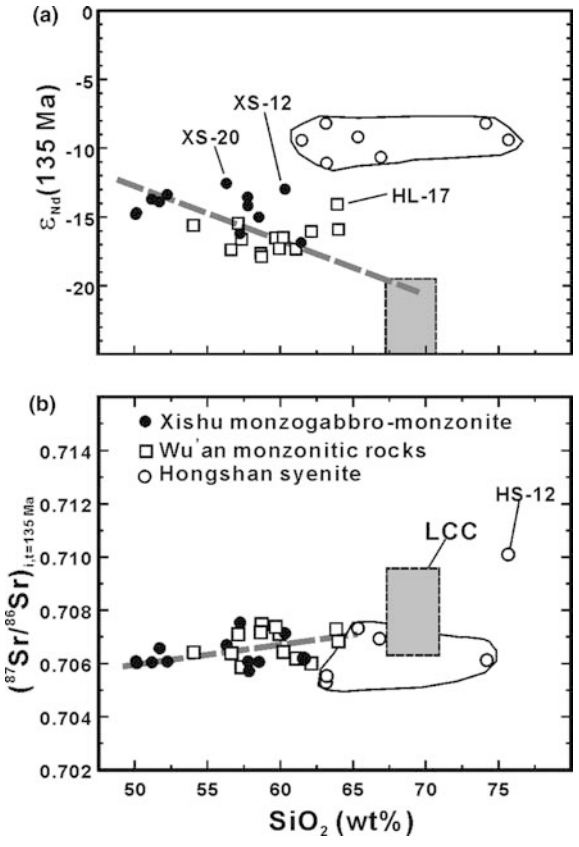

Fig. 8 Plots of **a** ε_{Nd}(135 Ma) vs. SiO_2, and **b** I_{Sr} vs. SiO_2, showing negative correlation of ε_{Nd} and positive correlation of I_{Sr} with increasing SiO_2 for the Xishu–Wu'an suites and lateral trends for Hongshan suite. HS-12 is ignored in **b** due to its large uncertainty of calculated I_{Sr}. Field of LCC is from Jahn et al. (1988)

the enriched SCLM source beneath the area is typically of EM1-type, with $\varepsilon_{Nd}(135\ Ma) = -8.2$ and $I_{Sr} = 0.7054$–0.7058. These isotopic compositions are significantly different from those of the Xishu rocks, indicating a significant contamination of these rocks by the lower crust. As shown in Fig. 6a, the Xishu rocks plot dispersedly between the EM1 source and LCC, reflecting variable degrees of contamination by LCC. The Wu'an rocks also plot between the EM1 mantle source and LCC, with data points distributing slightly farther away from the EM1 field than Xishu rocks, and more contamination by LCC is implied. Specifically, the ε_{Nd}(135 Ma) and I_{Sr} of the Xishu–Wu'an rocks are roughly inversely correlated (Fig. 6a), pointing to an important lower crustal incorporation. The scatter of data points is probably caused by the isotopic heterogeneity of LCC. Fan et al. (1998) suggested that the Mesozoic lower crust beneath the NCC was likely a mixture of Archaean TTG ($\varepsilon_{Nd} = -30$; Jahn et al. 1988) and Mesozoic underplated "basaltic" rocks ($\varepsilon_{Nd} = -8$ to -15; Zhang et al. 2002; Chen et al. 2003) from enriched mantle sources. The important input of lower crustal components in the Xishu–Wu'an rocks is evidenced by the linear evolution lines in plots I_{Sr} vs. 1/Sr (Fig. 7a) and ε_{Nd}(135 Ma) vs. 1/Nd (Fig. 7b), which evolve from the EM1 source to LCC.

Plots of SiO_2 vs. ε_{Nd}(135 Ma) (Fig. 8a) and SiO_2 vs. I_{Sr} (Fig. 8b) are used to further evaluate the role of LCC contamination. A roughly negative correlation is observed in Fig. 8a, whereas a positive trend is seen in Fig. 8b. Again, this indicates a significant contamination of the Xishu–Wu'an rocks by LCC. Samples XS-20, XS-12 and HL-7 plot off the evolution line in Fig. 8a, which may be attributed to contamination by the coeval Hongshan suite that has significantly higher ε_{Nd}(135 Ma) values, or, to the LCC's isotopic heterogeneity as discussed above. The Xishu rocks show higher ε_{Nd}(135 Ma) values than the Wu'an rocks (Fig. 8a), which, together with their lower silica contents, suggests a lower proportions of LCC components in them. Isotopic modeling was conducted based on an AFC model of DePaolo (1981; see Fig. 6a for parameters used) assuming the EM1 mantle ($\varepsilon_{Nd}(t) = -8.5$, $I_{Sr} = 0.7055$; Chen et al. 2003; Chen and Zhai 2003) and the LCC ($\varepsilon_{Nd}(t) = -30$, $I_{Sr} = 0.710$; Jahn et al. 1988) as two end-members. The result suggests 15–30% LCC contamination for the Xishu rocks, and 20–35% for the Wu'an rocks (Fig. 6a).

This model also agrees with our Pb isotopic data. As seen in Fig. 6, the data points of Xishu–Wu'an suites form linear variation between the EM1-type mantle and LCC fields; the Xishu rocks show slightly higher Pb isotopic ratios than the Wu'an rocks. Thus, the Xishu–Wu'an suites could have originated from partial melting of EM1-type mantle sources, but variably contaminated by LCC components en route to crustal levels.

Petrogenesis of Hongshan syenite–granites

The chemical variation trends (Fig. 3) of the Hongshan syenite–granites suggest they are genetically linked. In Fig. 3, kinks are observed at $SiO_2 = \sim 65\%$ in plots of SiO_2 vs. CaO, MgO, Al_2O_3, FeO, $K_2O + Na_2O$, and, to a lesser extent, TiO_2. This can be interpreted by a two-stage fractionation process. The earlier stage is characterized by fractionation of ferromagnesian phases (e.g., pyroxene and hornblende), producing the syenites, as is inferred from the negative relationship of SiO_2 vs. CaO, MgO and TiO_2. Feldspar removal is negligible during this stage, because Al_2O_3 is positively correlated with SiO_2 (Fig. 3), and, particularly, all syenites show minor to positive Eu anomalies (Fig. 5c). The later stage fractionation is probably dominated by a combined removal of feldspar and hornblende, producing the granites. This is suggested by the sharp depletion of Al_2O_3, TiO_2 and Sr with increasing SiO_2 (Fig. 3, 4). The important hornblende removal is indicated by granites' concave-shaped REE patterns with minor Eu anomalies (Fig. 5c), because hornblende removal tends to counteract the negative Eu anomaly caused by feldspar removal and result in middle REE depletion as well. Fractionation of apatite could also have partially con-

tributed to the middle REE depletion. Granites' LREE depletion (compared with syenites) probably reflects removal of allanite with large distribution coefficient for LREE. To prove this, we conducted a REE modeling based on the Rayleigh fractionation law. Sample HS-14 was chosen to represent the parental magma to granites. As shown in Fig. 5c, the calculated REE compositions of a residual melt after 22% fractionation of a cumulate assemblage of hornblende 51% + plagioclase 21% + K-feldspar 25% + apatite 1.7% + allanite 1.1% from the syenitic magma roughly match those for the granites (see legend of Fig. 5c for bulk distribution coefficients of the cumulate). Thus, the granites represent residual melts after a significant differentiation of syenitic magma. This is supported by the comparable Nd isotopic compositions of the two (Fig. 6a).

Traditionally, Hongshan syenites were considered to form by fractional crystallization from the nearby Xishu–Wu'an monzonitic rocks (Huang and Xue 1990). However, this model is not supported by our new data. As shown in Fig. 6a, the Hongshan syenites have $\varepsilon_{Nd}(T)$ values significantly higher than those for the Xishu–Wu'an rocks. Taking into account the different evolution trends of the Hongshan rocks in Figs. 3 and 4, it can be concluded that the Xishu–Wu'an monzonitic rocks were unlikely parental to the Hongshan syenites. This is further disclosed in Figs. 7 and 8 that the Hongshan syenites do not lie on the extension defined by Xishu–Wu'an suites. Other authors (e.g., Deng et al. 1996) advocated that the syenites were derived from partial melting of lower crustal rocks at high pressures (over-thickened crust). However, recent experimental data by Litvinovsky et al. (2000) demonstrate that partial melting of quartzofeldspathic rocks in the over-thickened lower crust produces granitic melts with 72–73% SiO_2, rather than syenitic liquids. Similarly, the melting experiments of Montel and Vielzeuf (1997) on a wide range of crustal materials show that syenitic melts are unlikely to be produced directly by anatexis.

We note from the plot I_{Sr} vs. $\varepsilon_{Nd}(135\ Ma)$ (Fig. 6a) that the Hongshan syenites have Sr–Nd isotopic compositions comparable to the EM1-type mantle. Sample HS-17 almost falls in the field of the mantle source, and the remainder (except HS-12 with imprecise I_{Sr} ratio) plot on the extension toward the LCC field. Similarly, the data points of these rocks lie near the EM1 mantle source in Pb isotopic plots (Fig. 6b, c), with extension towards the LCC field. Therefore, we suggest that the parental magma (not exposed) of the Hongshan syenites-granites also originated from partial melting of the EM1-type mantle source from which the Xishu–Wu'an rocks were derived, but in a *separate* magmatic event and were much less contaminated by LCC than the latter. Isotopic modeling suggests that less than 10% LCC components has been incorporated in the Hongshan rocks (Fig. 6a). Actually many syenites were reported to originate from enriched mantle sources, or form via a process of hybridization between mantle-derived basaltic magmas and crustal materials, like the Bryansky syenite–granite suite from Russia (Litvinovsky et al. 2002) and the Mesozoic syenitic magmas from Namibia (Harris et al. 1999).

The evolution of the syenite–granite complex appears to occur in a system with involvement of only a small amount of LCC. This is compatible with the roughly lateral variation trends of Nd–Sr isotopic ratios with SiO_2 (Fig. 8). Although the parental magma (likely an alkali-rich basalt) to the syenites is not exposed, the isotopic signature of the EM1-type source could be approximately reflected by the isotopically most "primitive" sample HS-17, with $\varepsilon_{Nd}(135\ Ma) = -8.2$ and $I_{Sr} = 0.7052$. The mantle source must have long been enriched in incompatible elements prior to partial melting, as suggested by the rather low ε_{Nd} value, and high Sr (948 ppm) and Rb (342 ppm) of the sample. In addition, the sample has relatively low $(^{206}Pb/^{204}Pb)_i$ ratios (< 17.6), with high, positive $\Delta 8/4$ (> 70) and relatively low $\Delta 7/4$ values (2.7; Table 3). These isotopic signatures agree with an EM1 source, suggesting a long-term low-μ mantle source (low U/Pb), and their positive $\Delta 8/4$ values suggest a long-term high Th/U source. Mantle enrichment may be caused by interaction of normal mantle peridotite with (1) fluids derived from a subducting slab (Maury et al. 1992) or (2) volatile-rich melts migrated from the asthenosphere (McKenzie 1989). The depletion of HFSEs (Nb, Ti) of the "primitive" sample in the spidergrams (Fig. 5f) suggests that the mantle enrichment is subduction-related, which probably happened in the early to middle Proterozoic as suggested by its high Nd model age (1.52 Ga).

Implications for lithosphere thinning

Voluminous Mesozoic igneous rocks were emplaced in East China. Their origin and the relationship with the eminent loss of lithospheric mantle during Mesozoic times has long been a disputed issue. We proposed in previous papers (Chen et al. 2002a, b, 2003; Chen and Zhai 2003) that enriched SCLM could be the main source for the Mesozoic magmas. The proportion of lower crustal material involved in their genesis was considered as less than 35% based on isotopic modeling; they thus represent significant addition of juvenile continental crust in Mesozoic times. This model is supported by our new data as well as some recent works (e.g., Qian et al. 2002). Therefore, the enriched mantle portions could be significantly consumed by melting to produce the Mesozoic magmas, triggered by upwelling of asthenosphere. This, together with thermo-mechanical and chemical erosion within the gradually upward moving lithosphere–asthenosphere interface, played an important role in thinning the lithosphere (Menzies et al. 1993; Xu 2001). The residual lithospheric mantle could be penetrated by, and mixed with, hot and dense asthenosphere, and then be removed through delamination.

Geodynamic setting

What is the cause of the sudden surge of magmatism in the Mesozoic? A popular model holds that the lithospheric destruction was related to the loss of physical integrity of the craton, caused by the Triassic collision between the NCC and Yangtze block (Menzies et al. 1993; Xu 2001; Gao et al. 2002). The Mesozoic magmatism was thus considered by many (e.g., Zhang et al. 2002; Mao et al. 2003) as post-collisional magmatism developed in an intra-continental extensional regime. We alternatively suggest that the Mesozoic magmatism was probably related to subduction of the paleo-Pacific slab based on the following two pieces of evidence: (1) The *earliest* Mesozoic intrusion in the Jiaodong Peninsula (easternmost margin of the NCC; inset of Fig. 1) was dated at ~170 Ma (zircon U–Pb; Wang et al. 1998) although many younger intrusions with ages ranging from 157 to 120 Ma are also present in the area. However, the magmatism in the Taihang orogen happened in a short time span from 138 to 125 Ma (Davis et al. 1998; Cai et al. 2003; Peng et al. 2004), with the earliest intrusion emplaced at ~138 Ma. A younging trend of magmatism from ~170 Ma in coastal area to ~138 Ma in inland NCC is thus noted, suggesting an inlandward movement of continental arc magmatism. This is consistent with the context of the northwestwards subduction of the paleo-Pacific slab beneath East Asia, which started in late Triassic (Arakawa and Shinmura 1995). And (2) The Mesozoic magmatic belts in the NCC are NE-trending (inset of Fig. 1), approximately parallel to the subduction zone (Maruyama 1997). Moreover, these rocks show strong arc magma signatures (Wang et al. 1998; Chen et al. 2002b). This model is particularly supported by the extensive accretion of arc complexes in the eastern margin of the East Asian continent during Jurassic times (Maruyama 1997). Taking into account previous work that the Mesozoic magmatism in NE China (Wu et al. 2003) and SE China (Zhou and Li 2000; inset of Fig. 1) was linked to the subduction of the paleo-Pacific slab, we propose that entire Eastern China is part of the East Asian continental arc, a model also advocated by Sengor and Natal'in (1996).

The genesis of the Mesozoic magmatism in southern Taihang can be described briefly as below. Subduction of the paleo-Pacific slab beneath the East Asian continent transformed the eastern part of NCC into an active continental margin. As a consequence, a back-arc extensional setting was developed in Taihang area (Fig. 1). This, in turn, induced the upwelling of asthenosphere. Meanwhile, fluids released from subducting slab penetrated and interacted with the overlying enriched portions of SCLM, lowering the solidus significantly. This, in conjunction with the high heat flow from the asthenosphere, triggered intense melting of the enriched SCLM, producing voluminous basaltic magmas. These mantle-derived magmas underplated in the lower crust, followed by differentiation and some contamination of lower crustal components, generating the magmatic complexes in the southern Taihang orogen.

Conclusions

1. The Xishu and Wu'an suites show many similar geochemical features such as LREE-enriched REE patterns with minor to positive Eu anomalies, and highly enriched isotopic compositions, pointing to their co-magmatic origin. They originated from partial melting of an EM1-type mantle source, followed by a coupled fractionation of ferromagnesian phases and significant contamination by LCC. The Wu'an rocks are chemically more evolved and isotopically slightly more enriched than the Xishu rocks, reflecting more involvement of crustal components.
2. The Hongshan syenites–granites show higher ε_{Nd}(135 Ma) and Pb isotopic ratios than the Xishu–Wu'an rocks though their I_{Sr} ratios are similar. They were formed from a *separate* parental magma that also originated from the EM1-type mantle source, but with minor incorporation of lower crust components during magma evolution. The granites are residual melts from the syenitic magma via a feldspar–hornblende-dominated fractionation.
3. A back-arc extensional regime was developed in the eastern part of NCC responding to the subduction of the paleo-Pacific slab beneath East China. Fusion of the enriched SCLM portions was induced by upwelling of asthenosphere and infiltration of slab-derived fluids. This, along with mechanical and chemical erosion within lithosphere–asthenosphere boundary contributed to the Mesozoic lithosphere thinning.

Acknowledgements Chen is grateful to Qiao GS, Zhang RH and Chu ZY (Beijing), and to Nicole Morin (Rennes), for their assistance in isotope analysis. We thank B. Litvinovsky and H. Martin for their constructive comments that helped to improve the manuscript. This work is supported by a Chinese Academy of Sciences grant (KZCX-107), a Natural Science Foundation of China grant (No.40372033), and a JSPS invitation fellowship (Japan).

References

Arakawa Y, Shinmura T (1995) Nd–Sr isotopic and geochemical characteristics of two contrasting types of calc-alkaline plutons in the Hida Belt, Japan. Chem Geol 124:217–232

Arth JG (1976) Behavior of trace elements during magmatic processes—a summary of theoretical models and their applications. J Res US Geol Surv 4:41–47

Brooks CK, Henderson P, Ronsbo JG (1981) Rare earth element partitioning between allanite and glass in the Obsidian of Sandy Braes, northern Ireland. Mineral Mag 44:157–160

Cai JH, Yan GH, Chang ZS, Wang XF, Shao HX, Chu ZY (2003) Petrological and geochemical characteristics of the Wang'an complex and discussion on its genesis (in Chinese with English abstract). Acta Petrol Sin 19:81–92

Chen B, Zhai MG (2003) Geochemistry of late Mesozoic lamprophyre dykes from the Taihang Mountains, north China, and implications for the sub-continental lithospheric mantle. Geol Mag 140:87–93

Chen B, Jahn BM, Wei C (2002a) Petrogenesis of Mesozoic granitoids in the Dabie UHP complex, central China: trace element and Nd-Sr isotope evidence. Lithos 60:67–88

Chen B, Zhai MG, Shao J (2002b) Petrogenesis and significance of the Mesozoic North Taihang complex: major and trace element evidence. Sci China (D) 46:941–953

Chen B, Jahn BM, Zhai MG (2003) Sr-Nd isotopic characteristics of the Mesozoic magmatism in the Taihang-Yanshan orogen, north China craton, and implications for Archean lithosphere thinning. J Geol Soc Lond 160:963–970

Davis GA, Zheng YD, Wang C, Darby BJ, Zhang C, Gehrels G (1998) Geometry and geochronology of Yanshan Belt tectonics. In: Collected works of international symposium on geological science. Seismic Press, Beijing, pp 275–292

Deng JF, Liu HX, Zhao HL, Luo ZH, Guo ZF, Li YW (1996) The Yanshanian igneous rocks and orogeny model in Yanshan-Liaoning area, North China (In Chinese with English abstract). Geoscience 10:137–147

DePaolo DJ (1981) Trace element and isotopic effects of combined wallrock assimilation and fractional crystallization. Earth Planet Sci Lett 53:189–202

Fan QC, Liu RX, Li HM, Li N, Sui JL, Lin ZR (1998) Zircon ages and REE geochemistry of granulite enclaves from the Hannuoba basalts. Chin Sci Bull 43:133–137

Gao S, Rudnick RL, Carlson RW, McDonough WF, Liu Y (2002) Re–Os evidence for replacement of ancient mantle lithosphere beneath the North China craton. Earth Planet Sci Lett 198:307–322

Harris C, Marsh JS, Milner SC (1999) Petrology of the alkaline core of the Messum igneous complex, Namibia: evidence for the progressively deceasing effect of crustal contamination. J Petrol 40:1377–1397

Hart SR (1984) A large-scale isotope anomaly in the Southern Hemisphere mantle. Nature 309:753–757

Huang FS, Xue SZ (1990) Petrology and geochemistry of the Han-Xing intrusive complex: implications for its origin (In Chinese). Acta Petrol Mineral 9:40–45

Jahn BM, Auvray B, Shen QH, Liu, DY, Zhang Z, Dong YJ, Ye XJ, Zhang QZ, Cornichet J, Macé J (1988) Archean crustal evolution in China: the Taishan complex, and evidence for juvenile crustal addition from long-term depleted mantle. Precambrian Res 38:381–403

Jahn BM, Wu FY, Chen B (2000) Granitoids of the Central Asian Orogenic Belt and continental growth in the Phanerozoic. Trans R Soc Edinb Earth Sci 91:181–193

Litvinovsky BA, Steele IM, Wickham SM (2000) Silicic magma formation in overthickened crust: melting of charnockite and leucogranite at 15, 20 and 25 kbar. J Petrol 41:717–737

Litvinovsky BA, Jahn BM, Zanvilevich AN, Shadaev MG (2002) Crystal fractionation in the petrogenesis of an alkali monzodiorite-syenite series: the Oshurkovo plutonic sheeted complex, Transbaikalia, Russia. Lithos 41:97–130

Ma XY (1989) Lithospheric dynamics atlas of China (in Chinese). China Cartographic Publishing House, Beijing

Mao JW, Wang YT, Zhang ZH, Yu JJ, Niu BG (2003) Geodynamic settings of Mesozoic large-scale mineralization in North China and adjacent areas. Sci China 46:838–851

Maruyama S (1997) Pacific-type orogeny revised: Miyashiro-type orogeny proposed. Island Arc 6:91–120

Masuda A, Nakamura N, Tanaka T (1973) Fine structures of mutually normalized rare-earth patterns of chondrites. Geochim Cosmochim Acta 37:239–248

Maury R, Defant C, Joron MJ (1992) Metasomatism of the sub-arc mantle inferred from trace elements in Philippines xenoliths. Nature 360:661

McKenzie DP (1989) Some remarks on the movement of small melt fractions in the mantle. Earth Planet Sci Lett 95:53–72

Menzies MA, Xu YG (1998) Geodynamics of the North China Craton. In: Flower MFJ, Chung SL, Lo CH, Lee TY (eds) Mantle dynamics and plate interactions in East Asia. Geophysical Monograph: American Geophysical Union 27:155–165

Menzies MA, Fan WM, Zhang M (1993) Palaeozoic and Cenozoic lithoprobes and loss of >120 km of Archean lithosphere, Sino-Korean craton, China. In: Prichard HM, Alabaster T, Harris NBW, Neary CR (eds) Magmatic processes and plate tectonics. Geol Soc Spec Publ 76:71–81

Middlemost EAK (1994) Naming materials in the magma/igneous rock system. Earth Sci Rev 37:215–224

Montel JM, Vielzeuf D (1997) Partial melting of greywackes: Part II. Composition of minerals and melts. Contrib Mineral Petrol 128:176–196

Nash WP, Crecraft HR (1985) Partition coefficients for trace elements in silicic magmas. Geochim Cosmochim Acta 49:2309–2322

Peng TP, Wang YJ, Fan WM, Peng BX, Guo F (2004) SHRIMP zircon U-Pb geochronology of the diorites for the southern Taihang Mountains in Central North Interior and its petrogenesis (in Chinese with English abstract). Acta Petrol Sin (in press)

Qian Q, Chung SL, Lee TY, Wen DJ (2002) Geochemical characteristics and petrogenesis of the Badaling high Ba–Sr granitoids: a comparison of igneous rocks from North China and the Dabie-Sulu Orogen. Acta Petrol Sinica 18:275–292

Qiao G (1988) Normalization of isotopic dilution analyses—a new program for isotope mass spectrometric analysis. Sci Sin 31:1263–1268

Rapp RP, Watson EB (1995) Dehydration melting of metabasalt at 8–32 kbar: implications for continental growth and crust-mantle recycling. J Petrol 36:891–931

Sengor AMC, Natal'in BA (1996) Paleotectonics of Asia: fragments of a synthesis. In: Yin A, Harrison TM (eds) The tectonic evolution of Asia. Cambridge Univ Press, Cambridge, pp 486–641

Song Y, Frey FA, Zhi XC (1990) Isotopic characteristics of Hannuoba basalts, eastern China: implications for their petrogenesis and the composition of subcontinental mantle. Chem Geol 85:35–52

Sun SS, McDonough WE (1989) Chemical and isotopic systematics of oceanic basalts: implications for mantle composition and processes. In: Saunders AD, Norry MJ (eds) Magmatism in the Ocean Basins. Geol Soc Lond Spec Publ 42:313–345

Wang LG., Qiu YM, McNaughton NJ, Groves DI, Luo ZK, Miao L, Liu YK (1998) Constraints on crustal evolution and gold metallogeny in the northwestern Jiaodong Peninsula, China, from SHRIMP U–Pb zircon studies of granitoids. Ore Geology Rev 13:243–258

Wolf MB, Wyllie JP (1994) Dehydration-melting of amphibolite at 10 kbar: the effects of temperature and time. Contrib Mineral Petrol 115:369–383

Wu FY, Jahn BM, Wilde S, Lo CH, Yui TF, Lin Q, Ge WC, Sun DY (2003) Highly fractionated I-type granites in NE China (I): geochronology and petrogenesis. Lithos 66:241–273

Xu YG (2001) Thermo-tectonic destruction of the Archean lithospheric keel beneath the Sino-Korean craton in China: evidence, timing and mechanism. Phys Chem Earth (A) 26:747–757

Xu WL, Lin JQ (1991) Dunite enclave found in a diorite pluton in Han-Xing district, Hebei province (N China), and implications (in Chinese). Acta Geol Sinica 65:33–41

Zhang HF, Sun M, Zhou XH, Fan WM, Zhai MG, Yin JF (2002) Mesozoic lithosphere destruction beneath the North China Craton: evidence from major-, trace-element and Sr-Nd-Pb isotope studies of Fangcheng basalts. Contrib Mineral Petrol 144:241–253

Zhou XM, Li WX (2000) Origin of late Mesozoic igneous rocks in southeastern China: Implications for lithosphere subduction and underplating of mafic magmas. Tectonophysics 326:269–287

Zhu BQ (1991) Evidence of isotopic systematics from crust and mantle for chemical heterogeneities of terranes. Chin Sci Bull 36:1279–1282

Zindler A, Hart SR (1986) Chemical geodynamics. Ann Rev Earth Planet Sci 14:493–571